Electronic Supplementary Information (ESI)

Well-organised two-dimensional self-assembly controlled by *in-situ* formation of a Cu(II)-coordinated rufigallol derivative: a scanning tunnelling microscopy study

Yoshihiro Kikkawa,[a]* Mayumi Nagasaki,[a] Seiji Tsuzuki,[a] Thierry Fouquet,[a] Sayaka Nakamura,[a] Yasumasa Takenaka,[b] Yasuo Norikane,[a] and Kazuhisa Hiratani[a]

[a] *National Institute of Advanced Industrial Science and Technology (AIST), Tsukuba Central 5, 1-1-1 Higashi, Tsukuba, Ibaraki 305-8565, Japan*

[b] *Bioplastic Research Team, RIKEN Center for Sustainable Resource Science, 2-1 Hirosawa, Wako, Saitama 351-0198, Japan*

1. Experimental details

Chemicals were purchased from Sigma–Aldrich, Kanto Chemical, Kishida Chemical, or Tokyo Chemical Industry and were used without further purification. The prepared compounds were characterised by ^{1}H and ^{13}C NMR spectroscopy (Bruker Avance 400 or 500 NMR spectrometer) using tetramethylsilane as the internal standard, and Fourier-transform infrared (FTIR) spectroscopy (JASCO FT/IR 420) using the KBr pellet method. High-resolution matrix-assisted laser desorption/ionization time-of-flight mass spectrometry (HR-MALDI-TOF-MS) was performed using a JMS-S3000 MALDI spiral TOF-MS instrument, with *trans*-2-[3-(4-tert-butylphenyl)-2-methyl-2-propenylidene]malononitrile (DCTB) as the matrix.

Preparation of rufigallol (1,2,3,5,6,7-hexahydroxy-9,10-anthraquinone)

Rufigallol was prepared by a previously reported method.[S1] Gallic acid (13 g) was dissolved in sulfuric acid (30 mL) and stirred at 100 °C for 6 h followed by stirring at room temperature (25 °C) overnight. After cooling, the solution was slowly poured into ice water (250 mL) with stirring. The precipitate was collected by filtration and washed three times with ice-cold water. After washing with *n*-hexane, the compound was dried at 50 °C overnight *in vacuo* to yield a dark red powder (6.45 g).

^{1}H NMR (500 MHz, DMSO-d_6): δ 7.24 (s, 2H), 9.93 (s, 2H), 10.74 (s, 2H), 12.93 (s, 2H).

Preparation of 1,5-dihydroxy-2,3,6,7-tetradodecyloxyanthraquinone (1)

Rufigallol (1 mmol) was dissolved in dry *N,N*-dimethylformamide (25 mL) and stirred with NaOH (4 mmol). Then, 1-bromododecane (4 mmol) was added, and the mixture was stirred at 100 °C overnight. The solvent was evaporated *in vacuo*, and the residue was extracted with $CHCl_3$ and dried over anhydrous $MgSO_4$. The crude product was purified by silica-gel column chromatography with $CHCl_3$ as the eluent and recrystallised from *n*-hexane to give an orange crystalline solid.

^{1}H NMR (500 MHz, $CDCl_3$): δ 0.88 (t, J = 6.65 Hz, 12H), 1.26 (br, 64H), 1.47 (m, 8H), 1.78 (m, 4H),

1.87 (m, 4H), 4.15 (t, J = 6.65 Hz, 4H), 4.18 (t, J = 6.45 Hz, 4H), 7.41 (s, 2H), 12.78 (s, 2H). ^{13}C NMR (100 MHz, $CDCl_3$): δ 14.1, 22.7, 25.9, 25.6, 29.1, 29.3, 29.4, 29.5, 29.61, 29.67, 29.72, 30.3, 31.9, 69.4, 73.8, 104.8, 111.8, 128.9, 141.2, 157.3, 158.0, 186.5. FTIR (KBr): 2954, 2918, 2849, 1618, 1602, 1570, 1507, 1468, 1419, 1362, 1327, 1281, 1227, 1142, 1092, 799, 721 cm^{-1}. HR-MALDI-TOF MS: *m/z* calculated for $C_{62}H_{104}O_8Na$, 999.7623 $[M+Na]^+$; found, 999.7620.

Preparation of 1-acetyl-5-hydroxy-2,3,6,7-tetradodecyloxy anthraquinone (2)

1,5-Dihydroxy-2,3,6,7-tetradodecyloxyanthraquinone (**1**, 1 mmol) and acetic anhydride (1 mmol) were dissolved in pyridine (10 mL) and refluxed with stirring overnight. The solvent was removed *in vacuo* and the crude product was purified by silica-gel column chromatography using 1:1 $CHCl_3$/hexane as the eluent to yield a yellow solid.

^{1}H NMR (500 MHz, $CDCl_3$): δ 0.88 (t, J = 6.90 Hz, 12H), 1.27 (br, 64H), 1.48 (m, 8H), 1.76 (m, 4H), 1.87 (m, 4H), 2.48 (s, 3H), 4.14 (m, 6H), 4.19 (t, J = 6.45 Hz, 2H), 7.33 (s, 1H), 7.73 (s, 1H), 12.89 (s, 1H). ^{13}C NMR (100 MHz, $CDCl_3$): δ 14.1, 21.0, 22.7, 25.92, 25.95, 25.99, 26.0, 29.01, 29.09, 29.30, 29.34, 29.38, 29.47, 29.51, 29.59, 29.61, 29.63, 29.68, 30.26, 30.33, 31.9, 69.3, 69.5, 73.7, 74.2, 104.9, 108.4, 111.4, 119.6, 130.0, 130.2, 140.4, 144.5, 146.4, 156.6, 157.2, 158.3, 169.1, 180.1, 186.4. FTIR (KBr): 2956, 2919, 2850, 1761, 1665, 1633, 1591, 1578, 1506, 1499, 1469, 1418, 1361, 1335, 1327, 1285, 1255, 1201, 1127, 1092, 780, 722 cm^{-1}. HR-MALDI-TOF MS: *m/z* calculated for $C_{64}H_{106}O_9Na$,1041.7729 $[M+Na]^+$; found, 1041.7731.

Preparation of 1,5-diacetyl -2,3,6,7-tetradodecyloxy anthraquinone (3)

1,5-Dihydroxy-2,3,6,7-tetradodecyloxyanthraquinone (**1**, 1 mmol) and acetic anhydride (4 mmol) were dissolved in pyridine (10 mL) and stirred while refluxing overnight. The solvent was removed *in vacuo* and the crude product was purified by silica-gel column chromatography using 1:1 $CHCl_3$/hexane as the eluent to yield a light-yellow solid.

^{1}H NMR (500 MHz, $CDCl_3$): δ 0.88 (t, J = 6.98 Hz, 12H), 1.27 (br, 64H), 1.48 (m, 8H), 1.76 (m, 4H), 1.88 (m, 4H), 2.48 (s, 6H), 4.07 (brs, 4H), 4.17 (t, J = 6.45 Hz, 4H), 7.65 (s, 2H). ^{13}C NMR (100 MHz, $CDCl_3$): δ 14.1, 21.0, 22.7, 25.96, 26.04, 29.01, 29.30, 29.38, 29.47, 29.59, 29.61, 29.68, 29.69, 29.71, 30.3, 31.9, 69.4, 74.1, 108.7, 118.8, 131.3, 143.9, 145.8, 157.3, 169.1, 180.1. FTIR (KBr): 2955, 2917, 2849, 1750, 1664, 1580, 1498, 1478, 1470, 1421, 1351, 1261,1235, 1198, 1113, 1092, 876, 781, 719 cm^{-1}. HR-MALDI-TOF MS *m/z* calculated for $C_{66}H_{108}O_{10}Na$,1083.7834 $[M+Na]^+$; found, 1083.7830.

Preparation of 1Cu and 2Cu (Metalated 1 and 2)

Either **1** or **2** (50 mg) was dissolved in a mixture of toluene (5 mL) and ethanol (10 mL), and a stoichiometric amount of copper(II) acetate was added. The mixture was stirred overnight at 80 °C. After cooling to room temperature, the product was collected by filtration and washed with a 1:2 toluene/ethanol solution. The metalated compounds were dried *in vacuo* at 50 °C to yield **1Cu** or **2Cu** as a purple or dark-magenta solid, respectively.

STM at the solid/liquid interface

The rufigallol derivatives (**1**–**3**) were dissolved in TCB at concentrations below 1 mM, while metalated compounds **1Cu** and **2Cu** were dissolved in TCB as much as possible by heating and sonication. Each saturated solution was deposited on a freshly cleaved HOPG surface, and the STM tip cut from a Pt/Ir wire (90/10: 0.25 mmϕ) was immersed in the solution. STM images were acquired at the HOPG/TCB interface with a scanning tunnelling microscope (Nanoscope IIIa, Digital Instruments). The HOPG lattice underneath the monolayer was used as the internal standard to correct STM images using SPIP software.

The *in-situ* STM experiment was performed as follows: copper(II) acetate was dissolved in alcohol (methanol, ethanol, propanol, or butanol) to a concentration of 20 mM, and the solution was

diluted with TCB to 1 mM. Compound **1** in TCB (1 mM) was deposited on the HOPG surface, and the copper(II) acetate solution was mixed on the substrate, after which the mixture was observed by *in-situ* STM at the HOPG/TCB interface. The type of alcohol did not significantly affect the experimental results.

2. Schematic diagrams of 2D structures

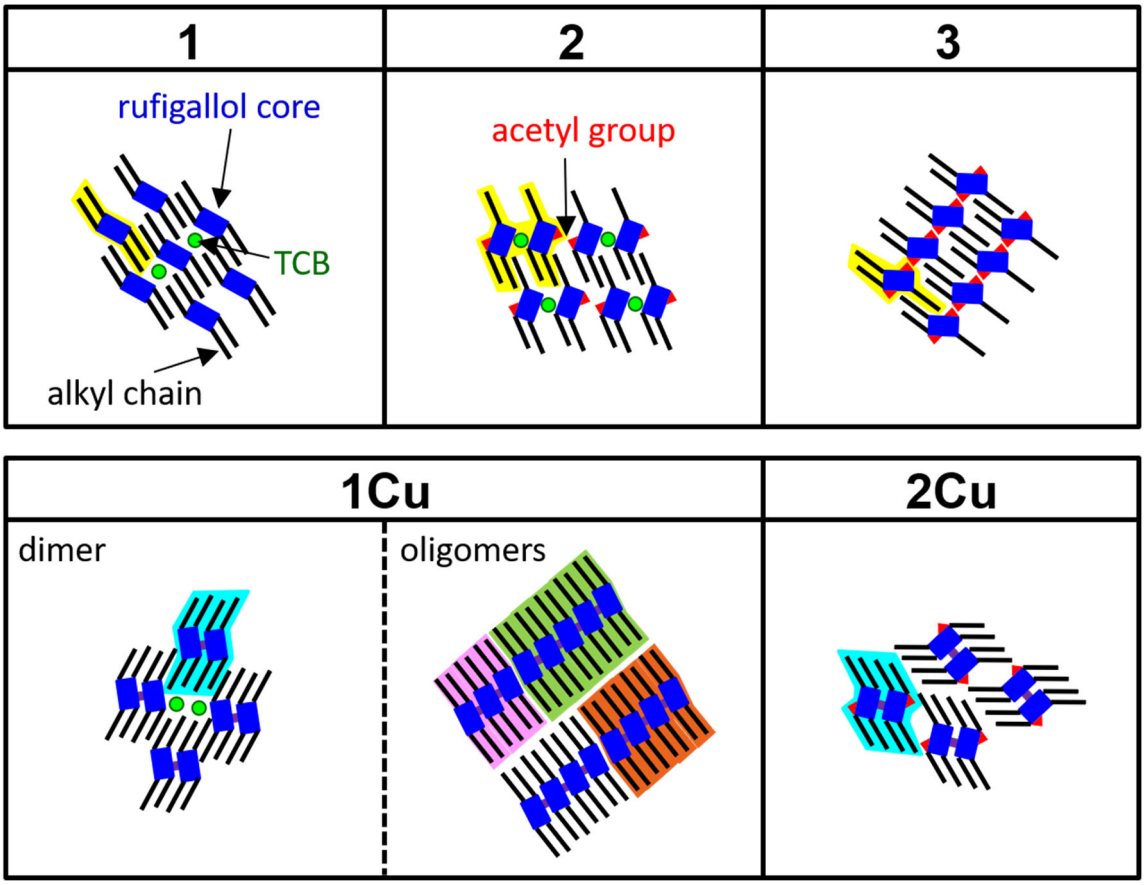

Fig. S1 Schematic diagrams of the 2D structures observed in this study. The repeating units of **1**–**3** are highlighted in yellow. The monomers, dimers, trimers, tetramers, and pentamers of metalated compounds **1Cu** and **2Cu** are highlighted in yellow, cyan, pink, orange, and green, respectively.

3. Additional STM images

STM images of 1–3

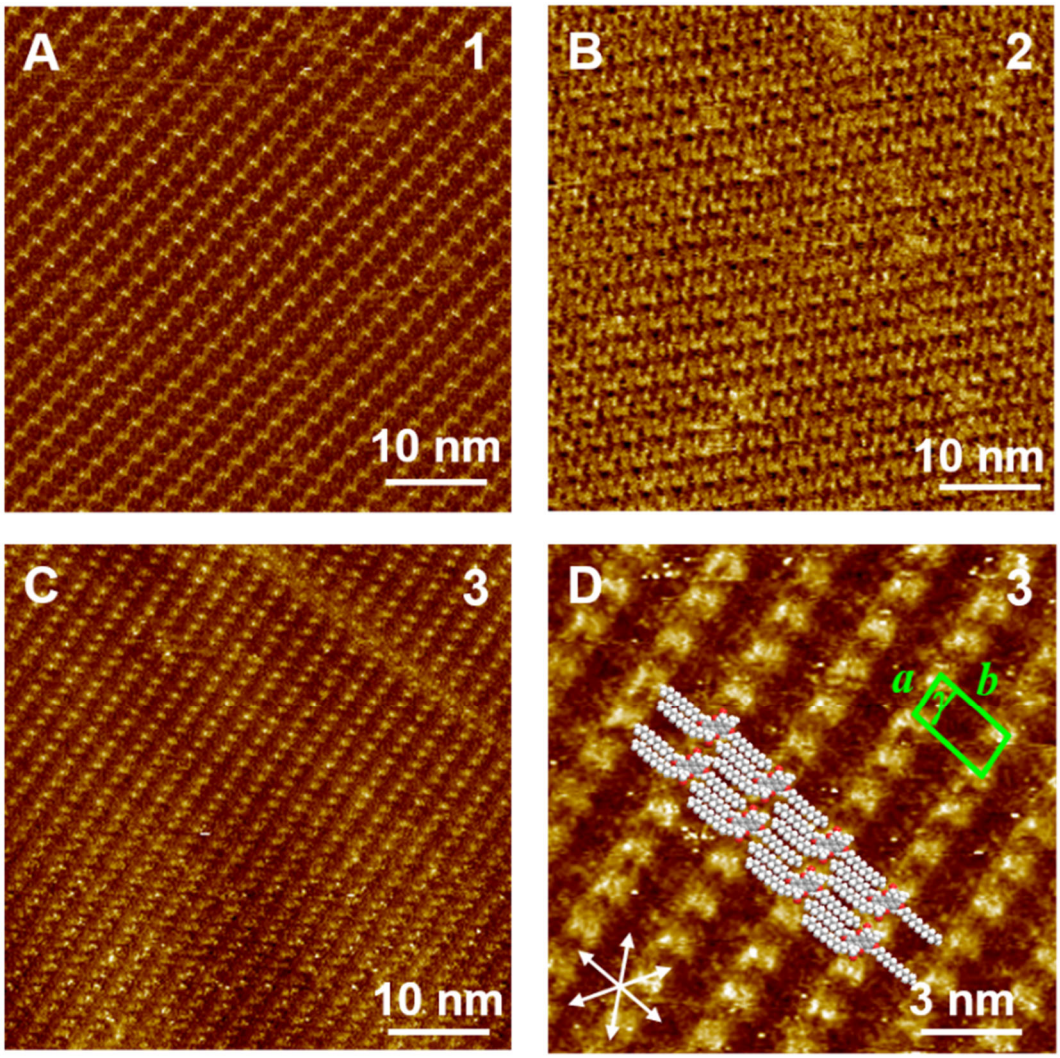

Fig. S2 STM images of rufigallol derivatives: (A) **1**, (B) **2**, and (C, D) **3** acquired at the HOPG/TCB interface. The set of arrows in the corner indicates the HOPG lattice directions. The proposed molecular model is drawn and overlapped on the STM image in (D). A schematic diagram of the 2D structure of **3** is shown in Fig. S1. Tunnelling conditions: (A) I = 50 pA, V = –827 mV; (B) I = 50 pA , V = –1200 mV.

STM images of 2Cu

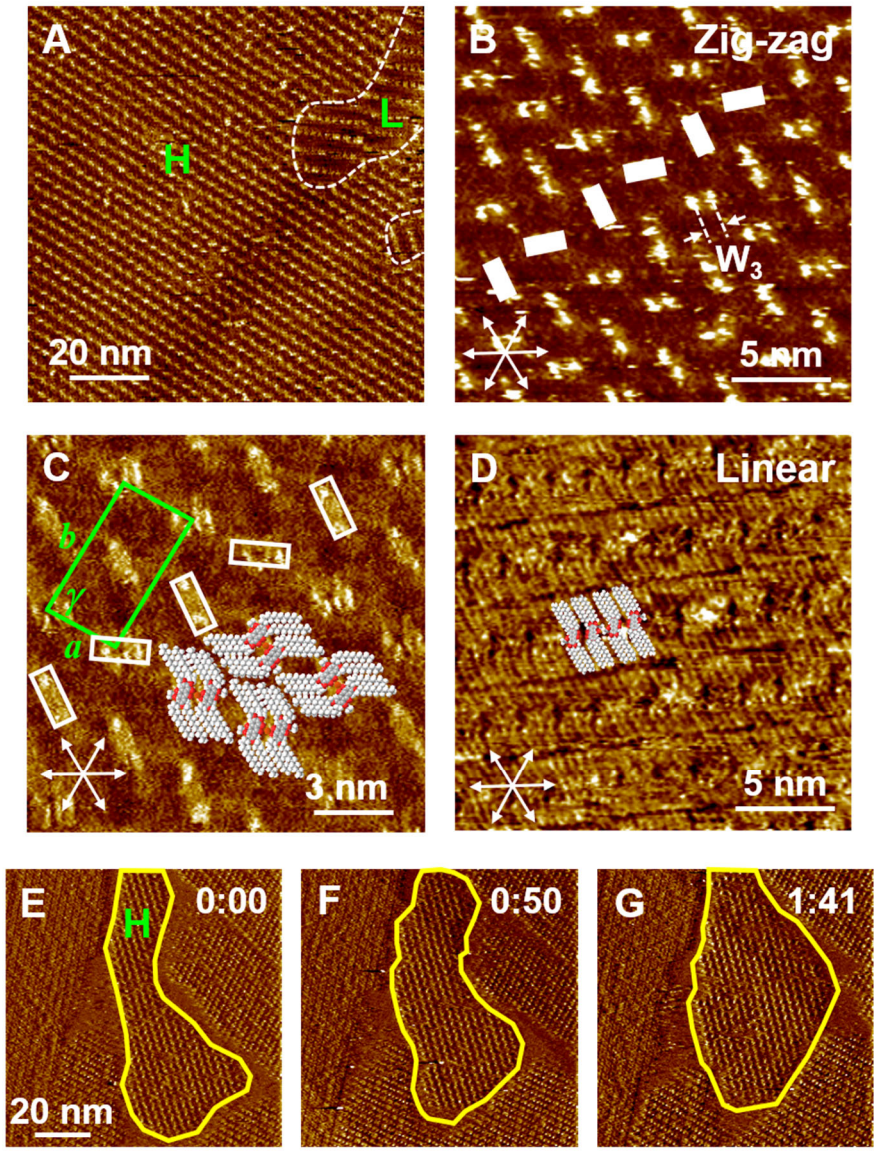

Fig. S3 STM images of rufigallol derivative **2Cu** acquired at the HOPG/TCB interface. The sets of arrows in the corners indicate the HOPG lattice directions. In (A), region H includes zigzag arrangements, whereas region L is composed of linear structures. In (B), white lines are drawn as a guide for visualising the zigzag arrangements. The distance between the **2Cu** (W_3) cores was measured to be 0.90 ± 0.09 nm, which is almost identical to the calculated distance between metalated rufigallol cores within error (see Fig. S9A). Panels (C) and (D) display STM images showing the zigzag and linear structures, respectively. Proposed molecular models are drawn and overlapped on the STM images. Panels (E)-(G) show consecutive STM images of **2Cu** prepared *in-situ* at the HOPG/TCB

interface. The area of region H (zigzag arrangements) increased with time, which is indicated at the right corner of each panel (min:sec). Note that the 2D structure of *ex-situ*-prepared **2Cu** (panel (A)) remained unchanged even upon addition of further of Cu(II) acetate on HOPG due to a lack of ligands with free coordination sites. STM images are acquisition times. Tunnelling conditions: (A) I = 35 pA, V = –400 mV; (B) I = 25 pA , V = –803 mV; (C) I = 25 pA, V = –609 mV; (D) I = 50 pA, V = –609 mV; (E-G) I = 30 pA, V = –166 mV.

STM images of the 1Cu dimer

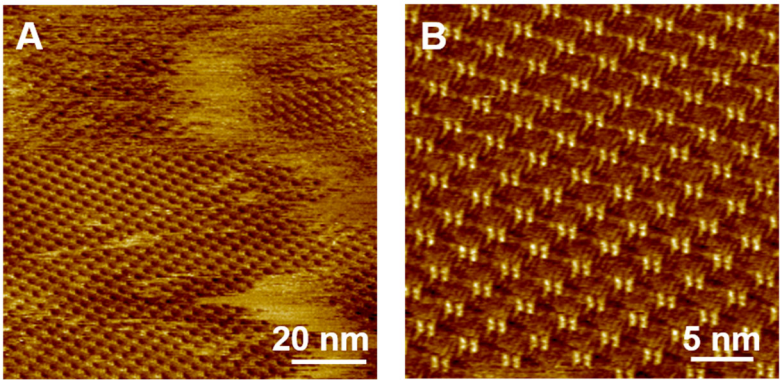

Fig. S4 STM images of the **1Cu** dimer at the HOPG/TCB interface. Tunnelling conditions: (A) I = 25 pA, V = –152 mV; (B) I = 25 pA V = –318 mV.

STM images of 1Cu oligomers (ex-situ)

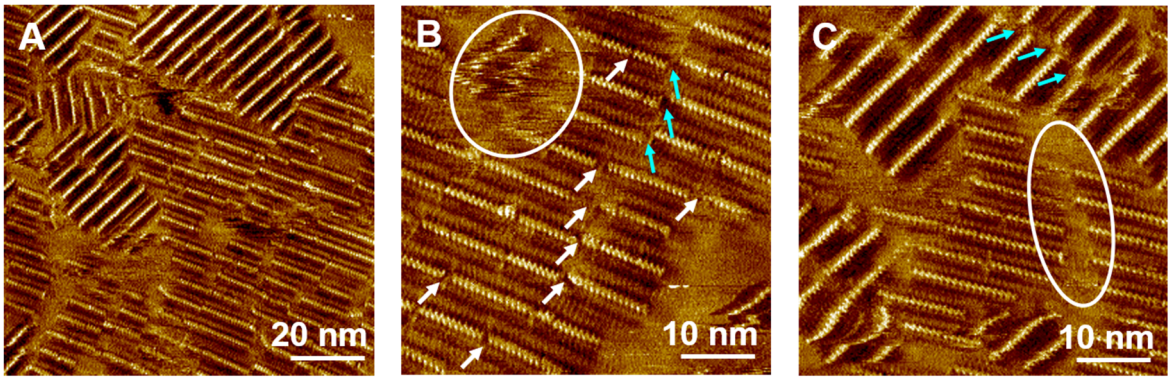

Fig. S5 STM images of *ex-situ*-prepared **1Cu**, showing defects (white arrows and ellipses) and slips (cyan arrows) along the column direction. Tunnelling conditions: (A-C) I = 50 pA, V = –700 mV.

STM images of 1Cu oligomers (in-situ)

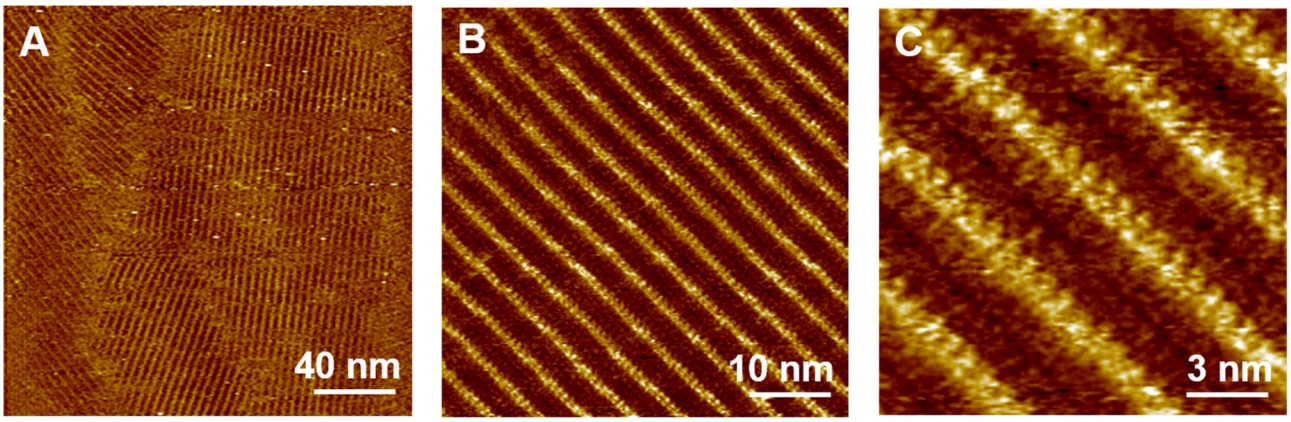

Fig. S6 STM images of *in-situ*-prepared **1Cu**, which exhibits regular molecular arrangements with continuous linear structures in the domain. Tunnelling conditions: (A) I = 25 pA, V = –827 mV; (B, C) I = 30 pA, V = –1000 mV.

Continuous STM images of 1Cu prepared in-situ

In some cases, the dynamic 2D structural-change process was observed using STM (Fig. S7). Domain structures were first observed after which ordered domains with linear arrangements increased in area (the outer areas enclosed by dotted cyan line in Figs. S7A–C). Finally, smaller domains with different orientations were assimilated withing the larger domain through Ostwald ripening[S1] (areas enclosed by yellow dotted lines in Figs. S7A–D) and became a well-ordered domain with an area of over 200 × 200 nm^2 (Fig. S7E).

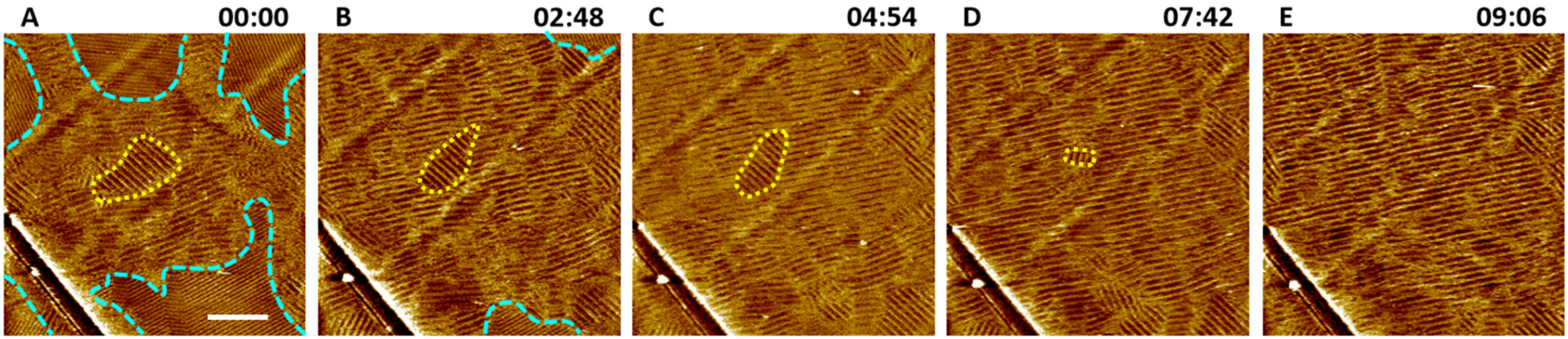

Fig. S7 Consecutive STM images of **1Cu** prepared *in-situ* at the HOPG/TCB interface. The regions enclosed by the cyan dotted lines are composed of the original 2D structure of **1**, whereas that enclosed by the yellow dotted line is the area that disappeared due to Ostwald ripening to form the regular 2D arrangement. Scale bar = 40 nm. Time (min: sec) above the STM images are acquisition times after panel (A) was acquired in a given region. Tunnelling condition: I = 30 pA, V = –1000 mV.

Addition of Cu(II) acetate to a TCB solution of ex-situ-prepared 1Cu on the HOPG surface

Cu(II) acetate in TCB was added to a TCB solution of *ex-situ*-prepared **1Cu** deposited on the HOPG surface, and the HOPG/TCB interface was observed by STM. Since **1Cu** is a mixture of oligomers, the molecular weight of the monomer unit in **1Cu** (Cu(II)-coordinated rufigallol) was tentatively used to calculate the concentration of the TCB solution. Figs. S8A–D show STM images of **1Cu** after the addition of one molar equivalent of Cu(II) acetate (**1Cu**:Cu(II) acetate = 1:1). Fig. S8A shows domain structures similar to those observed in Fig. 2A. However, continuous STM imaging revealed that the 2D arrays gradually disappeared after capturing the image in Fig. S8D. Since the amount of Cu(II) acetate relative to **1Cu** may be too high, **1Cu**:Cu(II)-acetate molar ratios of 3:1 and 10:1 were also examined. 2D structural changes due to metal coordination were also observed in both cases, with the self-assembled 2D structures also finally disappearing (e.g., Figs. S8E–H). Note that the addition of excess Cu(II) acetate to the *ex-situ*-prepared **1Cu** prior to deposition on HOPG led to an inability to observe 2D structures; hence, no images were obtained. These results suggest that further metal coordination of oligomerized **1Cu** affects its solubility in TCB, resulting in precipitation and an unstable 2D self-assembly at the solid/liquid interface.

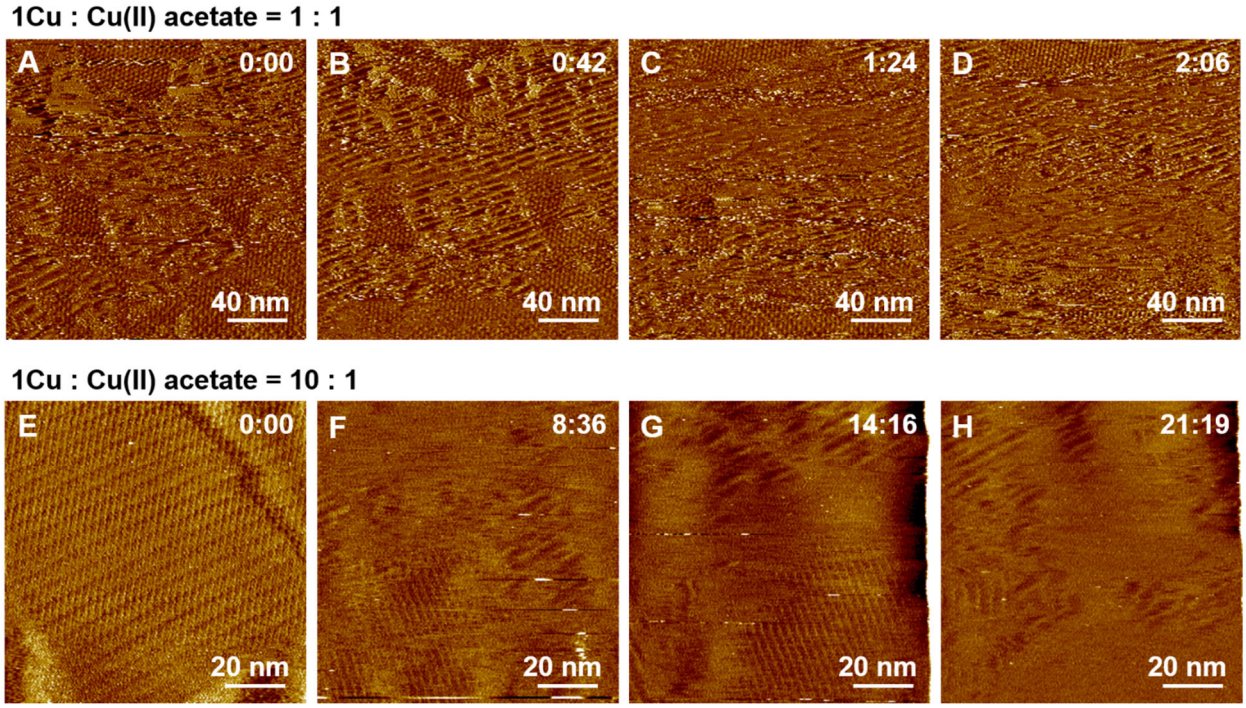

Fig. S8 Continuous STM images obtained after the addition of Cu(II) acetate to a TCB solution of *ex-situ*-prepared **1Cu** placed on the HOPG surface. The **1Cu**:Cu(II) acetate molar ratio was set to (A-D) 1:1 and (E-H) 10:1. The time (min:sec) at the top of each panel are acquisition times. No images could be obtained after observing panels (D) and (H). Tunnelling conditions: (A-D) I = 25 pA, V = –752 mV; (E-H) I = 25 pA, V = –909 mV.

4. Lattice constants

Table S1 Lattice constants of rufigallol derivatives of **1**–**3** measured from the STM images in Figs. 1 and S2.

	a (nm)	*b* (nm)	γ (deg)
1	1.77 ± 0.03	2.46 ± 0.08	74 ± 2
2	2.46 ± 0.06	3.07 ± 0.08	76 ± 2
3	1.36 ± 0.04	2.47 ± 0.04	81 ± 2

Table S2 Lattice constants of metalated rufigallol derivatives **1Cu** and **2Cu** measured from the STM images in Figs. 2 and S3.

	a (nm)	*b* (nm)	γ (deg)
1Cu_dimer	2.77 ± 0.03	3.14 ± 0.03	76 ± 1
1Cu_oligomer	0.86 ± 0.02	4.23 ± 0.10	88 ± 1
2Cu	3.00 ± 0.11	5.72 ± 0.06	87 ± 2

5. DFT calculations

DFT calculations were used to study plausible structures of the core parts of the rufigallol derivative dimers using the Gaussian 16 program.[S2] Geometries were optimized and interaction energies were calculated at the B3LYP/6-31G* level of theory[S3] with Grimme's D3 dispersion correction.[S4] Heavy atoms were kept coplanar during geometry optimization. Interaction energies were calculated with the BSSE[S5] correction using the counterpoise method.[S6] Fig. S9 shows the optimised structures of the metalated and hydrogen-bonded dimers of the rufigallol derivative, in which the dodecyloxy chain of **1** was replaced with a methoxy group. After metal coordination, the rufigallol derivative exhibited the molecular arrangement shown in Fig. S9A. Two orientations of the rufigallol core were generated for the hydrogen-bonded dimers: a parallel arrangement with intra- and intermolecular hydrogen bonds (Fig. S9B), and an oblique arrangement due to the Ar-H···O interaction in addition to intra- and intermolecular hydrogen bonds (Fig. S9C). The difference in the stabilisation energies of these orientations was calculated to be quite small (0.2 kcal/mol).

Linear and columnar **1Cu** structures are observed throughout the physisorbed monolayer in Figs. 2C and S4. Because **1Cu** is a mixture of oligomers with different degrees of metal complexation, the columnar structure must be composed of their assembly in a patch along the columnar axis. The optimised geometries of the dimers formed in Figs. S9B and S9C suggest that the oligomers in the column are connected not only through dispersion forces between the alkyl chains, but also through intermolecular hydrogen bonding. Indeed the dispersion interactions of dodecyl chains (~0.9 kcal/mol × 12 = 10.8 kcal/mol)[S7] are quite large compared to hydrogen bonding (~4.5 kcal/mol; see Fig. S9)) involving the rufigallol cores at the end of the oligomers; however, long columnar assemblies might be formed by the aggregation of oligomers supported by hydrogen bonding in a parallel arrangement (Fig. S9B). In addition, the column defects are possibly due to dislocations of dispersion interactions as well as the oblique arrangement of the rufigallol core through hydrogen bonding, as shown in Fig. S9C.

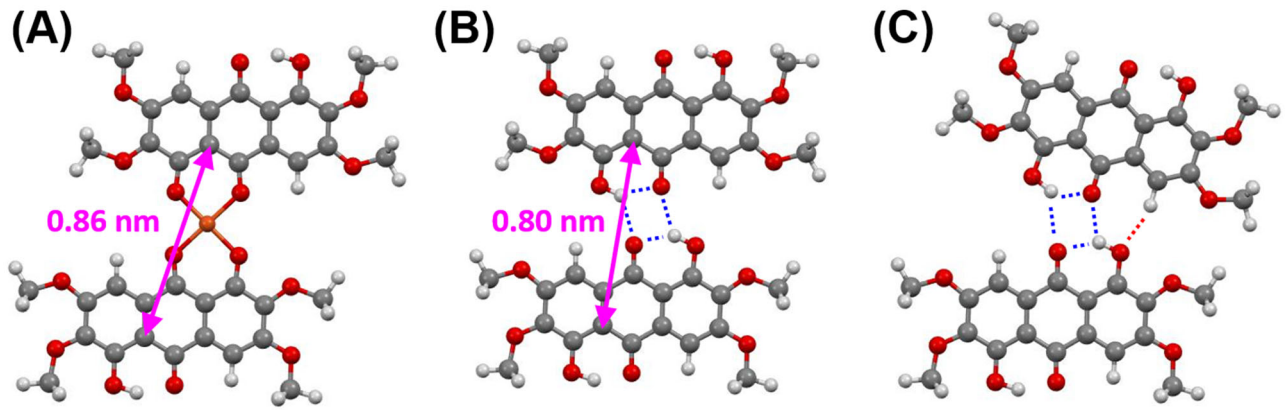

Fig. S9 DFT-optimised structures of the (A) copper(II)-coordinated and (B, C) hydrogen-bonded dimers of 1,5-dihydroxy-2,3,6,7-tetramethoxy anthraquinone. The stabilisation energies associated with the formation of the hydrogen-bonded dimers (the differences between the calculated energies of monomers and dimers) are: (B) −4.4 kcal/mol and (C) −4.6 kcal/mol. The blue dotted lines in (B) and (C) represent inter- and intramolecular hydrogen-bonding, whereas the red dotted line corresponds to the C-H···O interaction.

6. FT-IR spectroscopy

The non-metalated compounds (**1**–**3**) are orange-yellow in colour, whereas the metalated compounds (**1Cu** and **2Cu**) are purple. In addition to these colour differences, the FT-IR spectra before and after metal coordination with Cu(II) are also different (Fig. S10). The 1602 cm^{-1} band observed in Fig. S10A was less intense in Fig. S10B, and new peaks appeared at 1551 and 1500 cm^{-1}. In the case of **2** (Fig. S10C), new peaks at 1567 and 1508 cm^{-1}were observed for **2Cu** (Fig. S10D). These results suggest the formation of metal complexes.

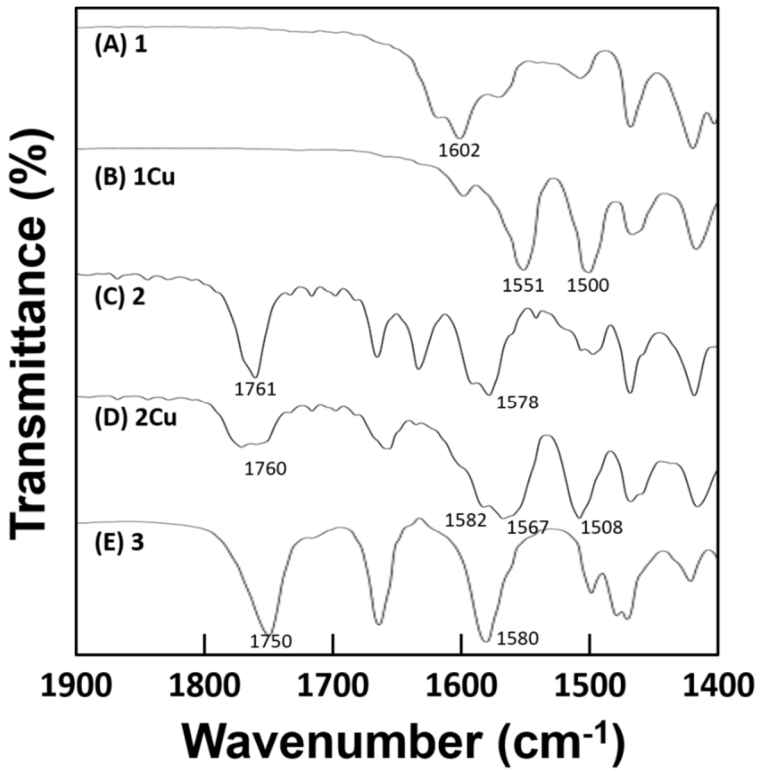

Fig. S10 FT-IR spectra of **1**–**3, 1Cu**, and **2Cu.**

7. MALDI-MS

MALDI-MS experiments were performed using the solvent free method. DCTB, sodium trifluoroacetate, and the sample powder were ground together using a mortar and pestle to prepare a homogeneous powder, which was deposited as a thin film on the MALDI target with a spatula. PMMA was used for internal calibration.

Fig. S11A shows the MALDI-MS spectrum of *ex-situ*-prepared **1Cu.** Several peaks indicative of oligomer formation are observed, despite the presence of unreacted monomer **1**, which suggests that **1Cu** is a mixture of oligomers with different degrees of metal coordination. As shown in Fig. S11B, most of the compound was converted into the metalated dimer **2Cu** although a small amount of monomer **2** was detected. Hence, the formation of the metal complexes of **1** and **2** were confirmed by combining FT-IR spectroscopy and MALDI-MS.

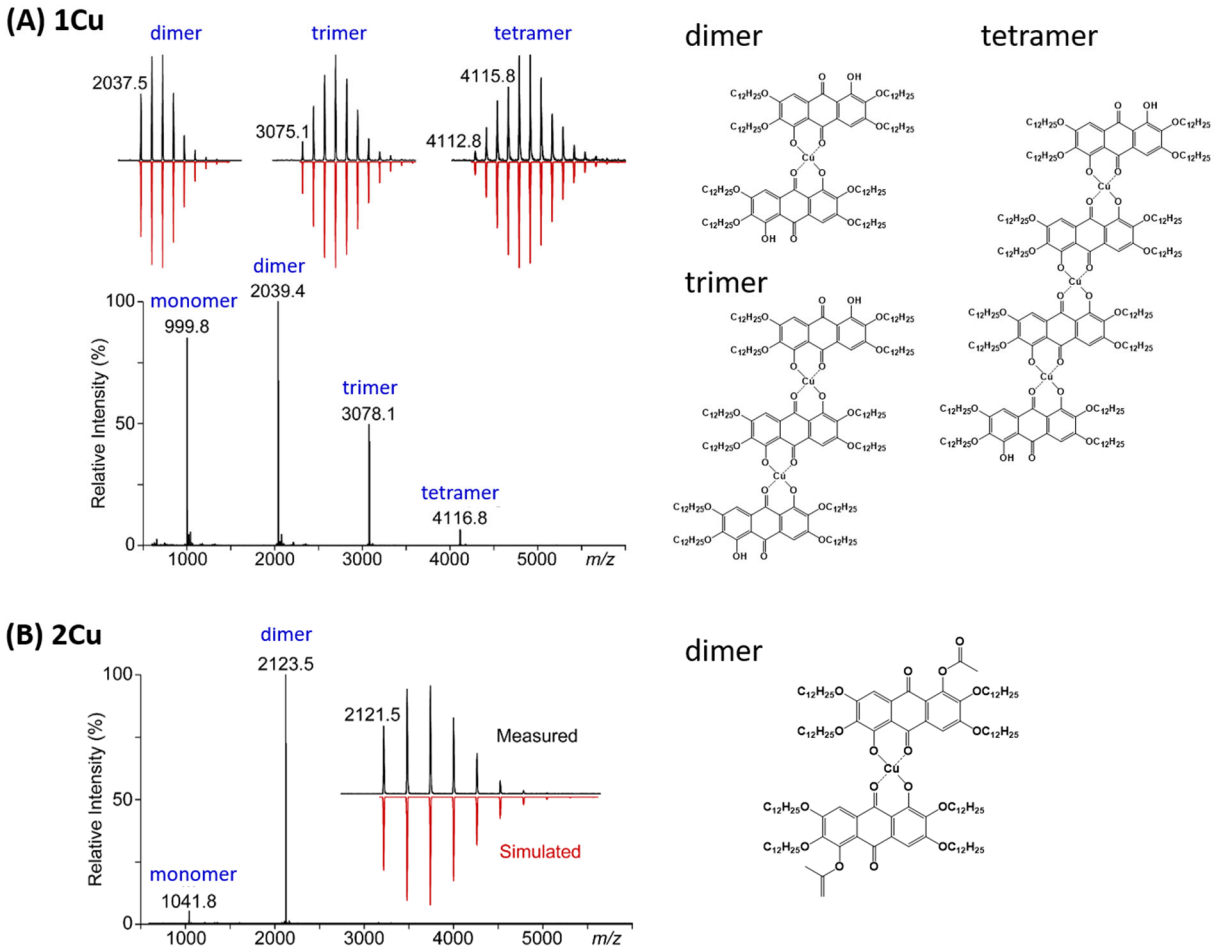

Fig. S11 MALDI-MS spectra of *ex-situ*-prepared (A) **1Cu** and (B) **2Cu.**

In addition, samples prepared under similar conditions to those used for *in-situ* STM were subjected to MALDI-MS. Compound **1** and Cu(II) acetate were separately dissolved in TCB to prepare 2.5 mM solutions, which were then mixed on HOPG and stored at room temperature (25 °C) for 1 h. After vacuum drying to remove the TCB, the remaining sample was scraped off with a spatula and subjected to MALDI-MS using the solvent-free method. Fig. S12A shows the MALDI-MS spectrum of **1Cu** prepared on HOPG. Oligomer species were detected in a similar manner to *ex-situ*-prepared **1Cu** (Fig. S11A). Note that a TCB solution of **1** and Cu(II) acetate mixed in a bottle also provided a similar MALDI-MS spectrum (Fig. S12B), suggesting that metal complexes are formed even when TCB is used as the solvent. Although it is impossible to distinguish between the products formed at the solid-liquid interface and in the solution phase, Fig. S12A suggests that oligomerised **1Cu** can be produced under the *in-situ* conditions.

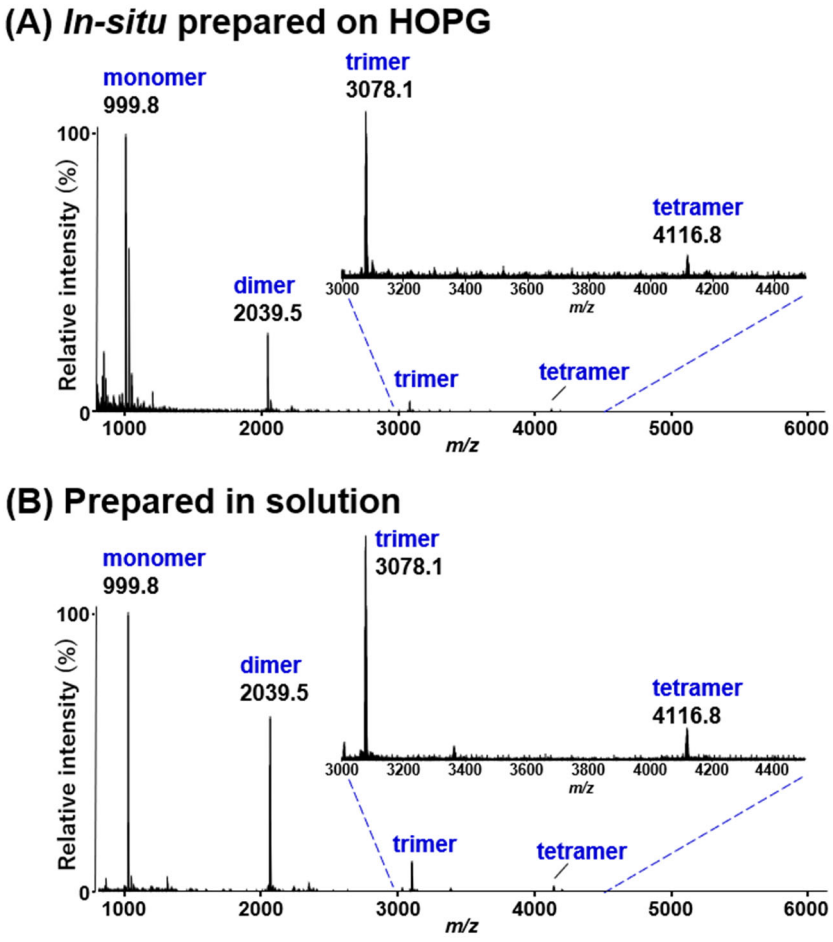

Fig. S12 MALDI-MS spectra of **1Cu** prepared (A) on HOPG and (B) in solution (bottle)**.**

8. Photographic images of 1 and 1Cu in TCB

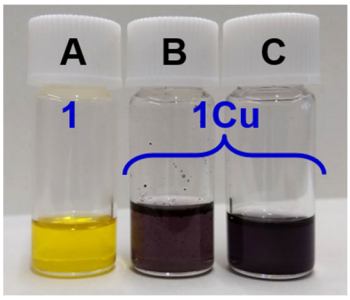

Fig. S13 Photographic images of (A) **1** and (B, C) **1Cu** dissolved in TCB. Vials (B) and (C) contain **1Cu** solutions that have been gently or vigorously sonicated and heated, respectively.

References

S1 For examples: (a) A. Stabel, R. Heinz, F. C. De Schryver and J. P. Rabe, *J. Phys. Chem.*, 1995, **99**, 505. (b) P. Samorí, K. Müllen and J. P. Rabe, *Adv. Mater.*, 2004, **16**, 1761. (c) T. K. Piskorz, A. H. De Vries, S. De Feyter and J. H. Van Esch, *J. Phys. Chem. C*, 2018, **122**, 24380.

S2 Gaussian 16, Revision C.01, M. J. Frisch, G. W. Trucks, H. B. Schlegel, G. E. Scuseria, M. A. Robb, J. R. Cheeseman, G. Scalmani, V. Barone, G. A. Petersson, H. Nakatsuji, X. Li, M. Caricato, A. V. Marenich, J. Bloino, B. G. Janesko, R. Gomperts, B. Mennucci, H. P. Hratchian, J. V. Ortiz, A. F. Izmaylov, J. L. Sonnenberg, D. Williams-Young, F. Ding, F. Lipparini, F. Egidi, J. Goings, B. Peng, A. Petrone, T. Henderson, D. Ranasinghe, V. G. Zakrzewski, J. Gao, N. Rega, G. Zheng, W. Liang, M. Hada, M. Ehara, K. Toyota, R. Fukuda, J. Hasegawa, M. Ishida, T. Nakajima, Y. Honda, O. Kitao, H. Nakai, T. Vreven, K. Throssell, J. A. Montgomery, Jr., J. E. Peralta, F. Ogliaro, M. J. Bearpark, J. J. Heyd, E. N. Brothers, K. N. Kudin, V. N. Staroverov, T. A. Keith, R. Kobayashi, J. Normand, K. Raghavachari, A. P. Rendell, J. C. Burant, S. S. Iyengar, J. Tomasi, M. Cossi, J. M. Millam, M. Klene, C. Adamo, R. Cammi, J. W. Ochterski, R. L. Martin, K. Morokuma, O. Farkas, J. B. Foresman, and D. J. Fox, Gaussian, Inc., Wallingford CT, 2016.

S3 A. D. Becke, *J. Chem. Phys.* 1993, **98**, 5648.

S4 S. Grimme, J. Antony, S. Ehrlich and H. Krieg, *J. Chem. Phys*. 2010, **132**, 154104.

S5 B. J. Ransil, *J. Chem. Phys*. 1961, **34**, 2109.

S6 S. F. Boys, F. Bernardi, *Mol. Phys*. 1970, **19**, 553.

S7 S. Tsuzuki, K. Honda, T. Uchimaru, M. Mikami, *J. Chem. Phys*. 2006, **124**, 114304.